AGU PUBLICATIONS

JGR

Journal of Geophysical Research: Oceans

RESEARCH ARTICLE
10.1002/2013JC009653

Special Section:
Western Pacific Ocean Circulation and Climate

Key Points:
- The East China Sea Kuroshio onshore intrusion shows interannual variability
- It is caused by the Kuroshio volume transport variability through axis shift
- Up and downstream of the intrusion area show antiphase interannual variations

Correspondence to:
F. Wang,
fwang@qdio.ac.cn

Citation:
Liu, C., F. Wang, X. Chen, and J.-S. von Storch (2014), Interannual variability of the Kuroshio onshore intrusion along the East China Sea shelf break: Effect of the Kuroshio volume transport, *J. Geophys. Res. Oceans*, *119*, 6190–6209, doi:10.1002/2013JC009653.

Received 25 NOV 2013
Accepted 5 AUG 2014
Accepted article online 8 AUG 2014
Published online 17 SEP 2014

Interannual variability of the Kuroshio onshore intrusion along the East China Sea shelf break: Effect of the Kuroshio volume transport

Chuanyu Liu[1,2], Fan Wang[1], Xinping Chen[3,4], and Jin-Song von Storch[5]

[1]Institute of Oceanology, Chinese Academy of Sciences, Qingdao, China, [2]Now at Institute of Oceanography, University Hamburg, Hamburg, Germany, [3]Institute of Oceanography, University Hamburg, Hamburg, Germany, [4]Now at National Marine Hazard Mitigation Service, State Oceanic Administration, Beijing, China, [5]Max-Plank Institute for Meteorology, Hamburg, Germany

Abstract The interannual variability of the Kuroshio onshore intrusion (KOI) across the East China Sea (ECS) shelf break and its response to the ECS Kuroshio volume transport (KVT) during 1993 ∼ 2010 are studied based on a high-resolution, real-time, and global ocean general circulation model. Since variability of KVT is mainly determined in the interior Pacific, it is rather a remote than a local factor for the local ECS KOI. On interannual time scales, KVT affects KOI not only in the net volume transport across the entire shelf break but also in the spatial pattern along the shelf break. When KVT increases, the intrusion decreases (increases) upstream (downstream) of the major intrusion region northeast of Taiwan, the retreating increases (decreases) upstream (downstream) of the main veering region southwest of Kyushu. These patterns are caused by cyclonic eddies induced by the seaward deflection of the Kuroshio axis from the shelf break, which ultimately results from the KVT increase. A diagnostic mechanism of $KOI \sim M \sin(\theta)|\nabla h^{-1}|$ is proposed, where h is the bottom depth, θ is the angle between isobaths and the vertically averaged current, and M is the absolute volume transport at the shelf break. θ is large in the major intrusion/retreating regions and stable on interannual time scales while M changes with opposite signs between upstream and downstream of the major intrusion/retreating regions. The mechanism explains well the relation of local KVT and the spatial pattern of KOI along the shelf break, in both the mean state and the interannual variations.

1. Introduction

The Kuroshio enters the East China Sea (ECS) east of Taiwan and leaves the ECS southwest of Kyushu (see Figure 1b for the geographic names). It exchanges extensively with the ECS shelf water, resulting in the intrusion of warm and saline Kuroshio water into the shelf, accompanied sometimes by intrusion of fresh and cold ECS shelf water into the Kuroshio. The regions northeast of Taiwan and southwest of Kyushu are two major onshore intrusion sources, which are long thought to be (partly) the origins of the Tsushima Warm Current [*Nitani*, 1972; *Isobe*, 1999; *Hsueh*, 2000; *Guo et al*., 2006; *Lee and Matsuno*, 2007]. The shoreward-seaward movement of the Kuroshio axis has been considered an agent of the Kuroshio onshore intrusion (KOI), which shows significant seasonal variability. Northeast of Taiwan, the Kuroshio in the upper layers tends to move farther away from the shelf in summer than in winter [*Sun*, 1987; *Tang et al*., 2000; *Liang et al*., 2003]. This seasonal migration was well summarized by *Sun* [1987], based on the 25 year geomagnetic electrokinetograph data. Southwest of Kyushu, the same electrokinetograph data identified a 50 km southward shift in summer relative to that in winter at 129° [*Sun and Su*, 1994]. The (summer) offshoreward shift of the Kuroshio northeast of Taiwan is often accompanied by the appearance of a cyclonic eddy and corresponding surface cold water centered at about 122.5°E, 25.5°N over the outer shelf, whereas the (winter) shoreward shift of the Kuroshio is often accompanied by a weakened cyclonic eddy, which remains mainly in the lower layers [e.g., *Su et al*., 1990; *Liu et al*., 1992; *Tang and Yang*, 1993; *Tang et al*., 2000; *Liang et al*., 2003; *Wu et al*., 2008; *Oey et al*., 2010]. The eastern part of the eddy brings water from the Kuroshio to the shelf, while the southwestward part of it, which locates close to the northeastern coast of Taiwan, brings water from shelf to the Kuroshio.

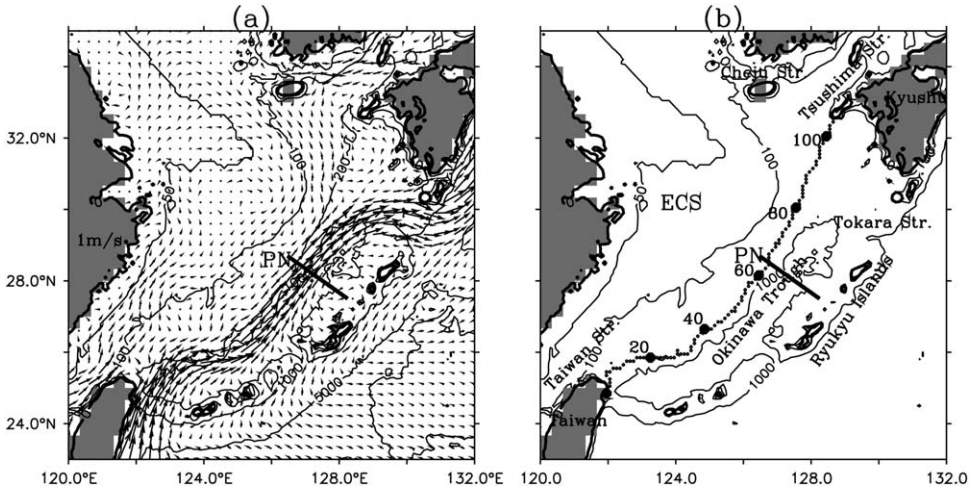

Figure 1. (a) The 18 year (1993–2010) mean of the simulated surface velocity in the ECS. The thick black line denotes the PN line; the contours are bottom depth (in m). (b) Geography of the study area. The small black dots along the shelf break is the model grid points at the 200 m isobath; the thick black dots are plotted every 20 grid points from Taiwan coast.

The shoreward-seaward shift of the Kuroshio axis is of big significance for the local physical and biochemical system [*Liu et al*., 1992; *Chen*, 1996; *Wong et al*., 2000], so that mechanisms for the cross-shelf shift attract much attention of the community. The local atmospheric forces have been demonstrated to contribute much to the Kuroshio axis shift, especially on seasonal time scales. *Oey et al*. [2010] demonstrated that a different along-isobath cooling rate northeast of Taiwan solely can induce the stronger intrusion in winter. Oey's work is a proof of *Tang and Yang*'s [1993] and *Chuang and Liang*'s [1994] anticipation that, northeast of Taiwan, wintertime cooling might be the major cause for triggering the strong winter intrusion event. *Guo et al*. [2003] demonstrated that, southwest of Kyushu, the summer (winter) southward (northward) shift is due to enhanced baroclinicity in summer relative to winter (cooling and strong wind stirring reduce the baroclinicity in winter). Overall, in these studies, the Kuroshio shoreward-seaward migration is explained by the joint effect of baroclinicity and bottom relief (JEBAR) [*Sarkisyan and Ivanov*, 1971], in which case the density inhomogeneity of the Kuroshio is caused by *local* atmospheric factors.

On the other hand, different mechanisms that might determine the variation of KOI were also mentioned in the literature. *Tang and Yang* [1993], using observations, hypothesized that the intrusion may also be related to "nonlocal" factors. *Guo et al*. [2003] and *Oey et al*. [2010] argued that the nonlocal factors should relate to the large-scale atmospheric pattern over the interior Pacific. Viewed from this perspective, the Kuroshio volume transport (KVT) might be considered as a nonlocal factor, because it is controlled by wind stress curl over and the density structure in [*Qiu and Chen*, 2010; *Chang and Oey*, 2011] the interior North Pacific. Since interannual variability of the upstream KVT has long been examined using both observations (e.g., *Gilson and Roemmich* [2002] based on XBT/XCTD data) and indirect estimations (e.g., by *Chang and Oey* [2011] based on altimetry and tide gauge data), concomitant interannual variability of KOI in the ECS is expected. This expectation can be confirmed by the year-to-year variability of the strength of the Kuroshio-induced cyclonic eddy and the cold dome northeast of Taiwan [*Tang et al*., 2000]. The objective of the present paper is therefore twofold: one is to identify the interannual variations of the KOI locally and of the entire ECS shelf break; the other is to investigate whether and how these variations are influenced by the interannual variations of KVT.

We are aware that the deviation of the mean Kuroshio axis from topography due to the special structures of coastal lines and bottom topography in the ECS is an important factor for the impinging of the Kuroshio onto the shelf. *Hsueh et al*. [1992], based on potential vorticity and mass conservation, interpreted the direction and volume transports of the onshore intrusion current in terms of both the upstream KVT and the incidence angle of the Kuroshio mainstream relative to the shelf break. A similar mechanism is also applicable to the Tsushima Warm Current southwest of Kyushu [*Hsueh et al*., 1996; *Lie et al*., 1998]. This factor will also be considered in the present study.

However, due to the lack of coordinating long-term and continuous observations of KVT and KOI covering the same region, a long-term comparison between KVT and KOI has not been possible from observations. Alternatively, simulations from a real-time, high-resolution, and global coverage general ocean circulation model with a realistic bathymetry are employed.

The remaining of the paper is organized as follows. A brief introduction of the numerical model and comparison of the model results to observations are given in the second section. Section 3 shows the interannual variability of KOI which is represented by cross-shelf break volume transport; the interannual variability of KVT is also described in section 3. The relation of interannual variations of KOI to KVT is discussed in section 4, and interpretation of the relation is made in section 5. Particularly, a newly proposed diagnostic mechanism is given in section 5. The paper ends with conclusions and discussions in section 6.

2. Model Descriptions and Validations

2.1. Model Descriptions

The simulation is performed with the Max-Planck Institute Ocean Model (MPIOM). It is formulated on a tripolar grid that was developed within the German consortium project STORM. The grid has a horizontal resolution of about 0.1°. It is curvilinear (Mercator) north (south) of the equator. The Mercator grid has a size of $0.1^\circ\cos(\varphi)$, where φ is latitude. Thus, the model has a resolution of 10 km at equator, and about 5 km or less south of 60°S. In the vertical, the model has 80 levels, with the thickness of the vertical layers increasing from 10 m in the first 100 m to about 280 m at the bottom. Apart from the grid, the model is based essentially on the same discretized primitive equations for a hydrostatic Boussinesq fluid, and has essentially the same physics and is coupled to the same sea ice model as its bipolar predecessor [*Jungclaus et al*., 2006]. The model is driven by the 6 hourly NCEP/NCAR reanalysis-1 [*Kalnay*, 1996] over the period 1948–2010 after a 25 year spin-up run. The outputs are monthly means. Detailed information on the STORM simulation can be found in von *Storch et al*. [2012].

2.2. The Simulated ECS Kuroshio and Observations

A preliminary examination of the model results revealed that the simulations become much closer to the observations in the ECS since year 1993 (not shown), which might be attributed to the improvement of the atmospheric forcing due to introduction of satellite measurements. Therefore, the results presented below are derived from years 1993 to 2010. The model simulations are compared with observations in terms of both long-term mean state of the Kuroshio and temporal variation of KVT. The 18 year (1993–2010) mean of the simulated surface velocity field in the ECS is shown in Figure 1a, which matches well the long-term electrokinetograph observation data [*Qiu and Imasato*, 1990, Figure 3]. It is seen that the most significant current in the ECS is the Kuroshio. The model also reproduces well the particular circulation structures in the two major intrusion regions. Northeast of Taiwan, part of the Kuroshio impinges onto the shelf as the Kuroshio branch current [*Qiu and Imasato*, 1990] (Figure 2c) and rejoins the Kuroshio mainstream further east (Figure 1a). A cyclonic eddy was seen, though not clearly, northeast of Taiwan. At around 127°E, 28°N∼30°N southwest of Kyushu, a branch-like current separates from the Kuroshio and flows northward (Figure 1a), feeding the Tsushima Warm Current [*Teague et al*., 2003]. At the same latitude, the main part of the Kuroshio loses control from topography and veers eastward to exit the ECS through the Tokara Strait.

The subsurface structures of the 18 year mean Kuroshio are shown along three typical sections (Figure 2). The PN section, where long-term continuous observations have been conducted, is located just before the Kuroshio veering region. Sections 122.5°E and 29°N are representative for the major intrusion region northeast of Taiwan and veering region southwest of Kyushu, respectively. The simulated cross-section velocity structure at the PN section agrees well with the long-term mean of observations [e.g., *Guo et al*., 2006, Figure 3]. A little difference is that the mainstream of the model Kuroshio is located in the upper layer (between 150 and 250 m), while the long-term mean of the observed Kuroshio shows a near-surface maximum. However, the modeled structure is often measured at and near the PN section [e.g., *Su et al*., 1990; *Ito et al*., 1995; *Ichikawa and Beardsley*, 1993]. The simulated density (Figure 2b), which reflects baroclinicity of the Kuroshio, also matches the observations. The accompanied vertical structure of velocity and the horizontal structure of density shown in Figures 2a and 2b are explained by the thermal wind relation. As will be discussed in the following sections, this geostrophic balance also holds in the cross-shelf break

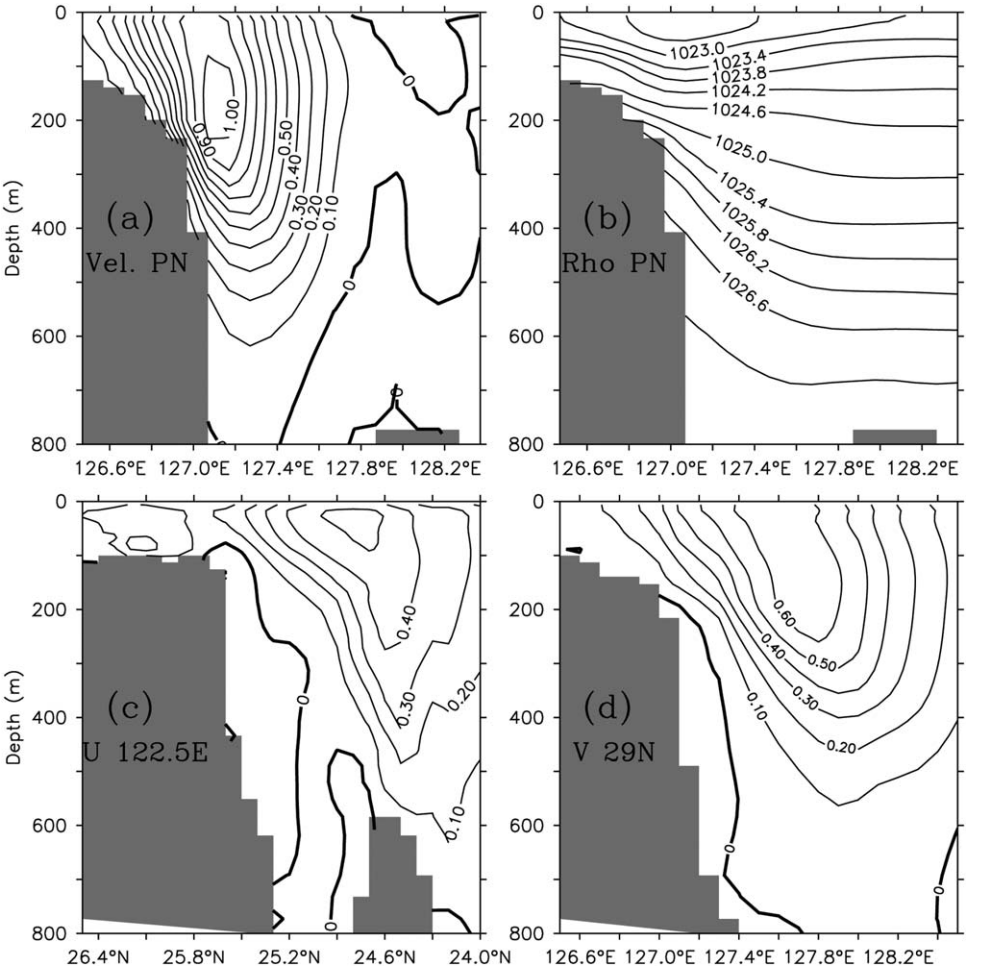

Figure 2. The 18 year (1993–2010) mean of the simulated (a) cross-section velocity (in m s^{-1}) and (b) density (in kg m^{-3}) at the PN section, cross-section velocity (in m s^{-1}) at (c) 122.5°E and (d) 29°N sections.

directions, establishing the relation between the along-isobath density gradient and cross-shelf velocity (i.e., KOI).

The model reproduced well the cyclonic circulations in the outer shelf northeast of Taiwan in the lower layers (below 100 m), which is indicated by weak westward and strong eastward velocities in between the Kuroshio branch current on the shelf and the main Kuroshio stream in the Okinawa Trough (Figure 2c). Studies mentioned in section 1 have revealed that this cyclonic eddy is a year-round phenomenon in the subsurface layers and may emerge on the surface in summer. A cyclonic eddy is also reproduced in the lower layers close to the shelf break at 29°N (Figure 2d), matching the observations [e.g., *Chen et al*., 1992, Figure 5]. The cyclonic eddies are all accompanied by the seaward deflection of the Kuroshio mainstream: the northward flowing Kuroshio east of Taiwan separates from the Taiwan coast to follow the zonally running topography, and it turns further eastward to separate from the shelf in the veering region.

The KVT across PN is obtained by vertically integrating the cross-section velocity from the surface to 800 m, a depth at which the Kuroshio vanishes (Figure 2). In general, the 1 year running mean of both the simulated and observed KVT are in good agreement in both magnitude and phase (Figure 3c). (The observational KVT used here is the same as used by *Zhang et al*. [2012], which was calculated from hydrographic measurements by the Nagasaki Marine Observatory of Japan, according to geostrophy and a reference level of no motion at 700 db.) For more details, spectra (wavelet) analysis [*Torrence and Compo*, 1998] on the 7 year high passed, 18 year monthly KVT shows variability of several significant periods, ~0.3, 1, and ~4 years at 95% confidence level (Figure 3a). A ~0.3 year (~100 days) peak is also evident in current-meter measurements in both upstream, i.e., east of Taiwan [*Zhang et al*., 2001] and downstream, i.e., in Tokara Strait [*Feng et al*., 2000], and is thought to be

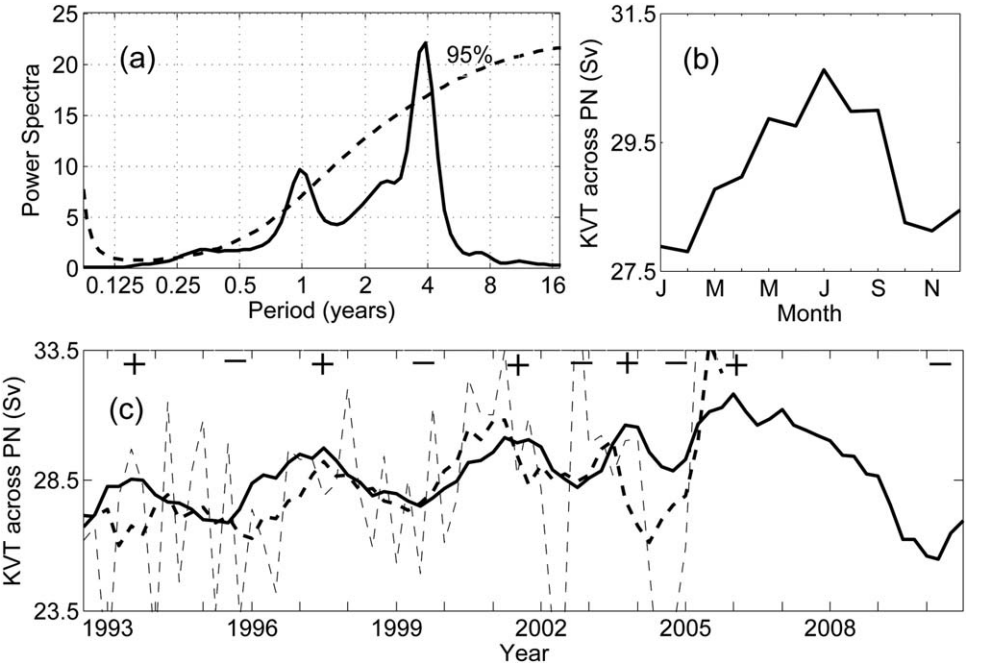

Figure 3. (a) Power spectrum of the 7 year high-passed monthly KVT (solid, unit is the variance of a certain period normalized by the variance of the entire time series) and the 95% confidence level (dashed). (b) Monthly climatology of the 18 year, simulated KVT. (c) Temporal variations of KVT across PN section (in Sv, 1 Sv = 10^6 m^3 s^{-1}): thick line is the 1 year running mean of the simulated monthly KVT, thin dashed line is the quarterly observational KVT, and thick dashed line is its 1 year running mean. The observational KVT after 2005 is not shown because of data unavailability. Symbols "plus" ("minus") at the top of Figure 3c denote months of KVT peaks (troughs) on interannual variations. The data process "1 year running mean" is practically made by using a 13-point running smooth centered on a given month with equal weights for months −5 to +5 and half weights for months −6 and +6.

related to the arrival of mesoscale eddies from the ocean interior [*Zhang et al*., 2001; *Ichikawa*, 2001]. The 1 year peak shows the annual cycle (seasonal variability). A monthly climatology of the present simulated KVT (Figure 3b) shows that the transport is high in summer (July) while low in autumn (Novermber) and winter (February). Observations have shown that the KVT across PN section is generally highest in summer and lowest in either autumn [e.g., *Hinata*, 1996] or winter [*Ichikawa and Chaen*, 2000], supporting our simulations. The interannual variation of ∼4 year period shows the ENSO scale of the Kuroshio variability, which is also found in other sections of the Kuroshio [e.g., *Saiki*, 1982; *Yamagata et al*., 1985; *He and White*, 1987; *Akimoto et al*., 1996; *Hwang and Kao*, 2002]. Overall, our simulation reproduces well the observed ECS Kuroshio in both of the long-term averaged spatial pattern and the temporal variations at different scales. In the remainder of the present study, we will focus on the interannual variability of the KVT (as well as the response of KOI to it).

3. Interannual Variability of the ECS KVT and KOI

3.1. Interannual Variation of the KVT

As in many previous studies, the KVT across PN section is selected to represent the ECS KVT. Both the model and observational KVT (Figure 3c) show relatively higher values in years of 1993, 1997, 2000–2001, 2003, and 2005–2006, while lower values in years of 1995, 1998–1999, 2004, and 2005–2008. The standard deviation (STD) of the 1 year running mean of the monthly KVT, which represents the amplitude of the interannual variation, is 1.4 Sv. The STDs of the 1 year running means, and of the deviations of the monthly KVT from the 1 year running means, which represent the total and seasonal/intraseasonal variations, are 2.2 and 1.7 Sv, respectively. The results suggest that the interannual variation has the same magnitude, as the total and seasonal/intraseasonal variations. As a factor of onshore intrusion as demonstrated in the following sections, the variation of KVT should be as important on interannual time scales as on seasonal time scales for the ECS KOI.

3.2. Long-Term Mean and Interannual Variation of KOI Across 200 m Isobath

The Kuroshio onshore flux is calculated by integrating the volume transport at each model grid point along the 200 m isobath, where the volume transport at each grid point is a vertical integration of the cross-

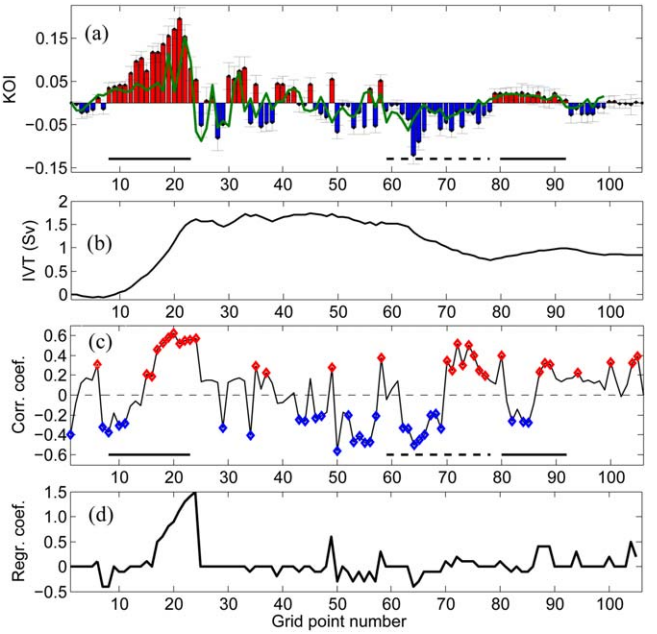

Figure 4. (a) The 18 year (1993–2010) mean of the Kuroshio onshore volume transport (in Sv) at each grid point along the 200 m isobath (color bars) and the corresponding STDs (error bars). The red (blue) bars denote net onshore (offshore) volume fluxes. Green line denotes the diagnostic estimation of KOI_{jebar} with equation (4), see text. Thick solid (thick dashed) lines at the bottom of plots (a) and (c) denote the major intrusion (retreating) regions. (b) The integrated Kuroshio onshore volume transport (in Sv) from the first grid point along the 200 m isobath. (c) Correlation coefficients between the 1 year running mean volume transport across the 200 m isobath at each grid point and the 1 year running mean KVT across PN section. Points with red (blue) diamonds denote significant positive (negative) correlation over 95% confidence level (±0.18). (d) Regression coefficients (in 10^{-2}) for points of significant correlation coefficients; it shows that the amount of positive change of KOI northeast of Taiwan (points 15–24) with unit change of KVT is larger than anywhere else, which explains the reason why the total KOI is positively correlated with KVT as shown in Figure 6. The grid points are shown in Figure 1b.

200 m isobath velocities at the point. The 200 m isobath (see Figure 1b for the locations of the grid points) is often chosen to represent the shelf break in studying the water exchange between ECS shelf and the ECS Kuroshio [*Guo et al*., 2006; *Lee and Matsuno*, 2007]. The 18 year averaged total volume flux across the 200 m isobath is 0.87 Sv, which is balanced mostly by the volume transport through the Tsushima Strait (2.57 Sv) and Taiwan Strait (1.85 Sv), and also by the southward volume transport through a section west of Kyushu (0.15 Sv). The simulated amount of transports through both Tsushima and Taiwan straits are among the ranges of previously observed and simulated results (see recent reviews by *Isobe* [2008] and *Yang et al*. [2011]). It is known that strengths of volume transport through the ECS shelf break and through both the Taiwan and Tsushima Straits influence the general circulation pattern of ECS [e.g., *Teague et al*., 2002; *Guo et al*., 2006]. Particularly, change of KOI at the shelf break might lead to smaller scale, local recirculations (such as the aforementioned cyclonic eddies). Therefore, a detailed investigation of the local pattern of both the mean KOI and its interannual variation along the shelf break is of great importance.

The 18 year averaged volume transport across the 200 m isobath at each grid point (Figure 4a, color bars) and along subsections according to local intrusion or retreating patterns (Figure 5) show that KOI takes place mainly northeast of Taiwan (points 7–23), while offshore flux takes place mainly in the retreating region where the Kuroshio separates from the shelf break (points 59–79). They provide 1.67 Sv onshore fluxes and 0.75 Sv offshore fluxes, respectively (Figure 4b). Immediately northeast of Taiwan (points 1–6), 0.07 Sv of shelf water intrudes into the mainstream of the Kuroshio, which corresponds to the seaward flowing limb of the year-round cyclonic eddy [*Chuang et al*., 1993; *Hsueh et al*., 1993; *Tang and Yang*, 1993; *Tang et al*., 1999, 2000].

For the interannual variability, the net KOI across the entire 200 m isobath also shows an interannual periodicity of $\sim$ 4 year period, which can be seen from the 1 year running mean (Figure 6): higher intrusions happen in years 1993, 2000–2001, 2003–2004, and 2005–2008 and lower intrusions happen in years 1994–1995, 1999, 2002, and 2009–2010, roughly in agreement with the years of higher and lower KVT, respectively. The STD of interannual variation is 0.24 Sv, which is nearly a half of the total STD (0.59 Sv). This implies that the interannual variation of KOI, like that of KVT, is of the same significance as seasonal/intraseasonal variations. Locality in interannual variations is also found along the 200 m isobath (Figure 7). The grid points can be divided into two subgroups according to the interannual variation patterns. For example, grid point 10 and grid point 20 roughly vary in antiphase: point 20 (10) shows positive (negative) intruding

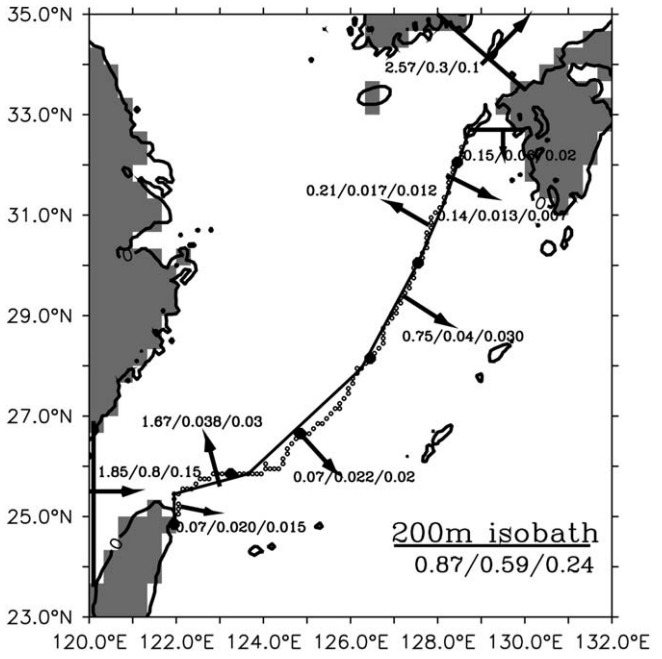

Figure 5. The 18 year (1993–2010) mean volume transport across particular sections and the corresponding STDs (in Sv) in the ECS. The three numbers for each section show the 18 year mean volume transport, the STD of monthly volume transport through each section, and the STD of the 1 year running mean volume transport through each section, respectively. The arrows represent the directions of volume transport. The transport and STD across the entire 200 m isobath are shown in the lower right corner.

anomalies, which means reduced (enhanced) intrusion, in years 1993, 1997–1998, 2001–2002, 2005–2008; in other years, negative (positive) anomalies are found. Anti-phase variations (though weak) are also found between grid points 60–70 and 71–80.

4. Relationship Between KOI and KVT on Interannual Time Scales

4.1. Relation of KOI Along the 200 m Isobath to KVT

The correlation coefficient between the 1 year running mean KVT and the total onshore flux across the 200 m isobath is 0.78 (at 99.9% confidence level). The regression coefficient is 0.14. Taking the KVT STD of 1.4 Sv on interannual time scales (see section 3.1), the regression coefficient 0.14 yields a cross-200 m isobath volume flux of $1.4 \times 0.14 = 0.20$ Sv in the absence of other processes, accounting for most of the interannual STD of the KOI (0.24 Sv). The positive correlation between the cross-200 m isobath onshore flux and KVT in the present study is also found from case experiments [*Lee and Matsuno*, 2007]. This clearly indicates that, on interannual time scales, KVT plays an important role in determining KOI along the entire ECS shelf break.

In order to identify the local pattern of the cross-shelf break onshore intrusion with a change of KVT, the correlations between the shoreward flux at each grid point and KVT are calculated (Figure 4c). A pronounced feature is that, within any of the major intrusion or retreating region, the responses of local KOI to KVT are generally opposite between upstream and downstream. (To ease the comparison, the major intrusion and retreating regions are denoted by thick solid and dotted lines, respectively, at the bottoms of Figures 4a and 4c, as well as Figures 12a and 14a.) For example, in the major intrusion region northeast of Taiwan (points 7–23), the KOI and KVT are negatively correlated at points 7–12, indicating reduced intrusion with increased KVT, while they are positively correlated at points 15–24, indicating enhanced intrusion with increased KVT. In the main retreating region (points 59–80), the KOI and KVT are negatively correlated

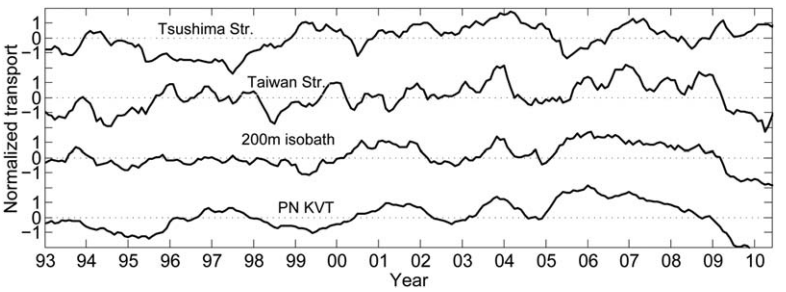

Figure 6. Monthly anomaly of the 1 year running mean volume transport relative to the 18 year mean (each is normalized by its STD). See their locations in Figure 5.

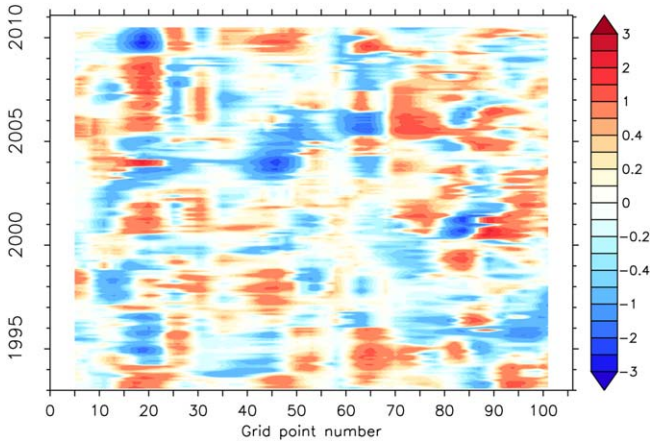

Figure 7. Time-grid points plot of the 1 year running mean volume transport anomalies (compared to the 18 year mean) at each grid point (in 10^{-2} Sv) along the 200 m isobath. The grid points are shown in Figure 1b. A five-grid point running mean is applied.

upstream (points 62–70), indicating that the retreating of the Kuroshio water from the shelf is enhanced with an increase of KVT here; however, they are positively correlated downstream (points 71–80), implying reduced retreating in the northern part of the separation region, with an increase of KVT in the further upstream. Similarly, in the other main intrusion region southwest of Kyushu (points 80–92), the intrusion increases (decreases) upstream (downstream) with an increase of KVT.

We note that the transport flux of each grid varies differently with change of the KVT. For example, it is shown in Figure 4d by linear regression coefficients that each grid in the positively correlated region northeast of Taiwan (points 15–24) contributes more than 1×10^{-2} Sv with one Sv change of KVT, while most grids in the negatively correlated region contribute about only one order smaller; totally, the intrusion overcomes the retreating and results in the positive relation of the total along 200 m isobath KOI to the KVT, as mentioned in the beginning of section 4.1 and shown in Figure 6. However, in the following sections, we focus on the local KOI processes rather than their quantities.

4.2. Relation of the Local KOI Processes to KVT

We first apply two diagnostic properties, APV and TPV (see Appendix A), to investigate the effect of KVT on the vertically averaged current field in the study area from a 2-D point of view. Briefly, APV and TPV represent volume transport across and along *f/h* contours respectively, where *f* is the Coriolis parameter and *h* is the bottom depth. The contours of *f/h* resemble the isobaths since *f* varies little in the study area.

The 18 year (1993–2010) averaged APV (Figure 8a) at the shelf break resembles the long-term mean pattern of the cross-200 m isobath volume transport (Figure 4a) very well: regions northeast of Taiwan (corresponding to grid points 7–24 of the 200 m isobath) and southwest of Kyushu (grid points 80–92) are the major sections providing the onshore volume transport, indicated by positive APV. The retreating region, where the Kuroshio separates from the shelf break and leaves the ECS (grid points 60–80), is the main place providing most of the offshore fluxes, indicated by negative APV. Its counterpart TPV (Figure 8c) displays well the generally northeastward flowing pattern along isobaths of the ECS currents, including the Kuroshio, the Taiwan Warm Current, and the shelf circulations. Particularly, the southwestward flowing countercurrent along isobaths northeast of Taiwan, which is denoted by negative TPV, represents the offshore part of the year-round cyclonic eddy as mentioned above.

The effect of ECS KVT on interannual variability of APV (TPV) at each point of the study area can be deduced by the correlation coefficients in Figure 8b (Figure 8d). The correlation pattern around the shelf break hence reveals more detailed 2-D structures than that shown in Figure 4c. Just along the 200 m isobath, APV and KVT are negatively correlated upstream of the major intrusion region northeast of Taiwan (points 7–15) and positively correlated downstream (points 16–25); however, seaward from the shelf break in this region, the coefficient between APV and KVT becomes negative both upstream and downstream (Figure 8b). Considering together the negative correlation just along the 200 m isobath and positive correlation seaward of it between TPV and KVT (Figure 8d), one may reasonably imagine that, with the increase of KVT, a counterclockwise eddy-like current anomaly may be generated here. This scenario is even clearer in the veering region (points 60–80).

We now apply the composite map to illustrate the detailed response of currents to KVT in Figure 9. This map gives the difference of the vertically averaged velocity between months of the highest and lowest 1

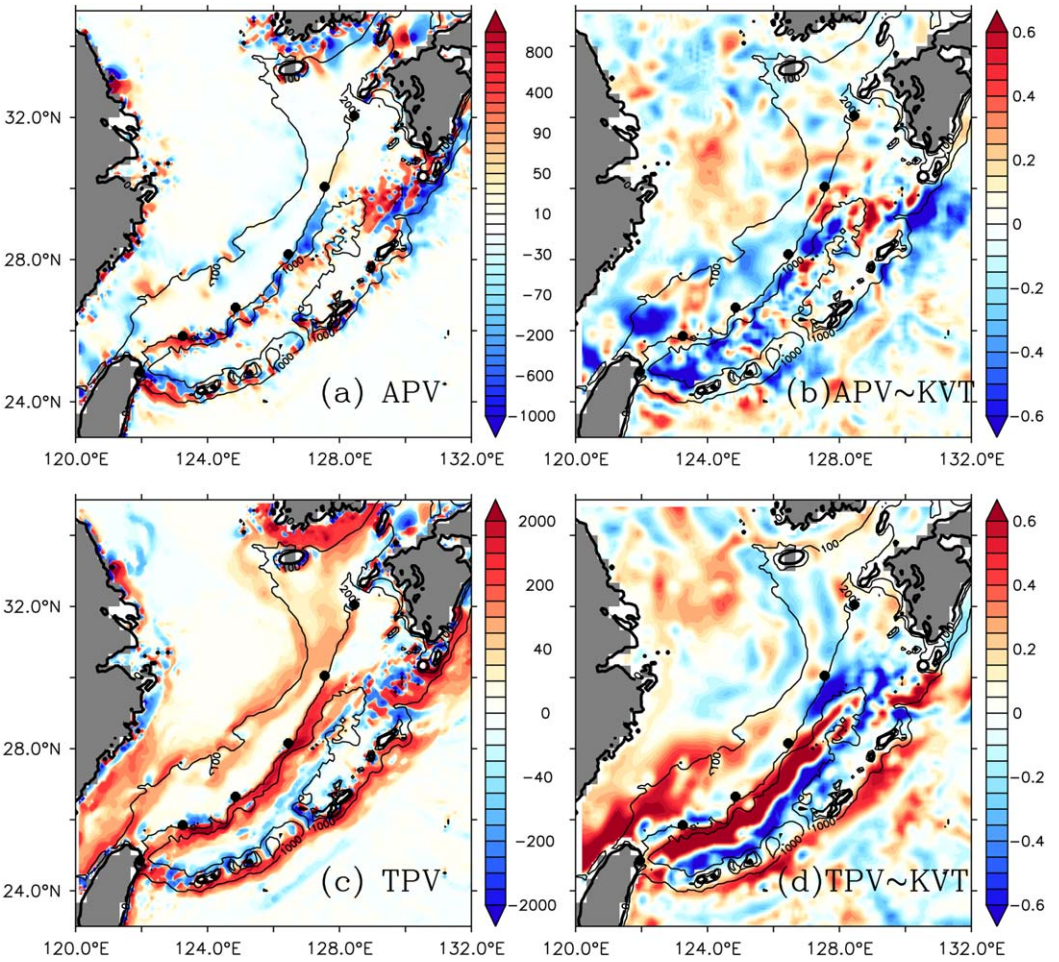

Figure 8. The 18 year mean of (a) APV and (c) TPV. Correlation coefficients between the 1 year running mean KVT and the 1 year running mean (b) APV and (d) TPV. See Appendix A for definitions of APV and TPV.

year running mean KVT, and indicates the velocity change tendency in accordance with KVT change. (See Figure 3c for the corresponding months.) Cyclonic eddy-like velocity differences emerge in both the outer shelf northeast of Taiwan (centered at about 122.6°E, 25.4°N, not to be confused with the anticyclonic eddy-like velocity difference centered at 122.0°E, 25.5°N) and the veering region southwest of Kyushu (centered at about 128.5°E, 29.5°N). Northeast of Taiwan, the northwestern (northeastern) part of the cyclonic eddy-like velocity difference, which flows southward (northwestward), is associated with the seaward intrusion between points 7–15 (shoreward intrusion between points 16–24) in Figures 4c, 8b, and 8d. Southwest of Kyushu, the southwestward (northeastward) flowing part of the cyclonic eddy-like velocity difference is associated with the shoreward intrusion between points 71–80 (seaward intrusion between points 59–70) in Figures 4c, 8b, and 8d. Observations have discovered that the cyclonic eddy northeast of Taiwan is a persistent phenomenon, i.e., it happens year-round though is weak in the upper layers in winter (Figure 2c) and varies intraseasonally and seasonally as mentioned before. The increase of KVT tends to strengthen it, and extends it from lower layers to surface layers, which is indicated by the southwestward current difference close to the coast and northeastward current difference on the outer side (Figures 10c and 10d). This tendency holds also for the cyclonic eddy in the veering region (Figure 10b), where a long-term mean weak cyclonic eddy also exists (Figure 2d). The cyclonic eddy-like velocity differences near the PN section and at other sections of the shelf break shown in Figure 9 become much squashed along the shelf break. Moreover, a shelf-scale cyclonic recirculation of the velocity difference that flows around the northwestern margin of the ECS Kuroshio emerged with an increase of KVT.

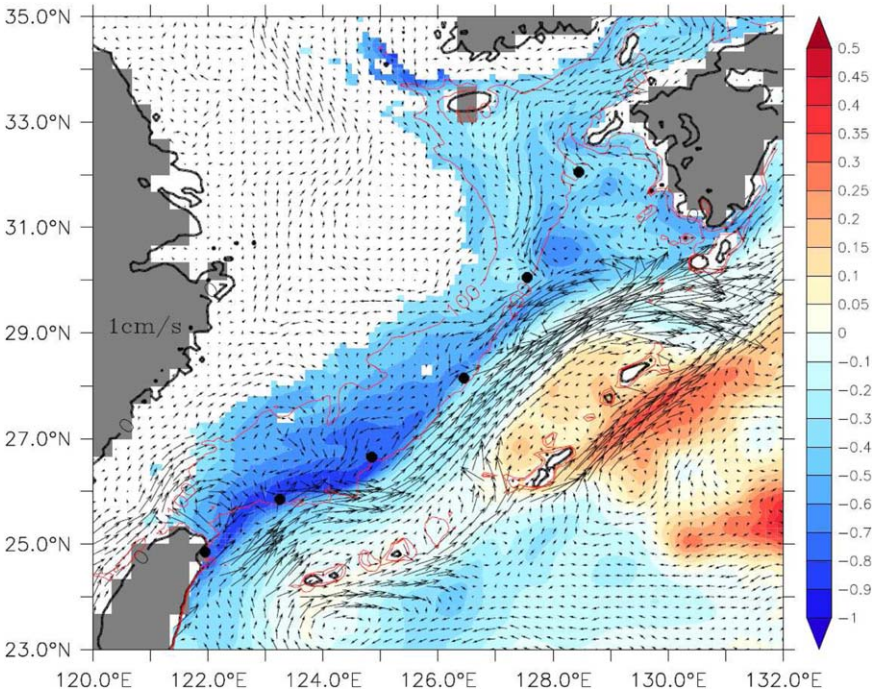

Figure 9. Difference of temperature (color, in °C) on 80 m depth and difference of vertically averaged velocity (arrows) between months of highest and lowest 1 year running mean KVT. The months of highest and lowest KVT are denoted with "plus" and "minus" symbols in Figure 3c.

We note that the eddy-like structures are tendencies of velocity changes associated with increase of KVT, and do not necessarily show up as real eddies. The tendencies can be summarized below: when KVT increases, the intrusion decreases and increases upstream and downstream, respectively, of the major intrusion region northeast of Taiwan; the retreating increases and decreases upstream and downstream, respectively, of the main retreating region southwest of Kyushu. Each of the regions is accompanied by a cyclonic eddy-like velocity change. Moreover, the entire ECS shelf break is also accompanied by a cyclonic recirculation of velocity difference. These eddy-like velocity changes are important for balancing the local KOI, which is discussed in the following section.

5. Mechanisms of the Interannual Variability of KOI

In this section, we aim to investigate how the increase of KVT leads to changes of the local KOI pattern on interannual time scales. We start with the generation mechanism of cyclonic eddies and corresponding upwelling, which is followed by an interpretation of the KOI mechanism from the JEBAR point of view. Consequently, we give a diagnostic equation that is formulated in terms of volume transport and the mean angle between the mean Kuroshio Current and isobaths.

5.1. How Does the Change of KVT Induce Changes of Local KOI?

5.1.1. The Kuroshio Axis Shift and the Generation of Upwelling/Cyclonic Eddies Due to Changes of KVT

The mean path of boundary currents passing curved bathymetric topography depends on its β-Rossby number, which is the ratio of the nonlinear inertial term to the linear planetary vorticity gradient term [*Vallis*, 2006, chapter 14.5] and/or Reynolds number [*Sheremet*, 2001], which is the ratio of nonlinear inertial terms to the viscosity terms. *Pierini et al*. [2011] found from laboratory study that, by increasing the western boundary current speed (inertia) the current transits from a pattern that follows the coast to a pattern that separates from the bathymetric cape. *Sheremet* [2001] argued that when a western boundary current passes a geographic gap, the dominative inertia (relatively high velocity) tends to make the current leap the gap; otherwise, the (relative slow) current will follow isobaths. The above studies essentially show the inertia feature of the western boundary currents [*Charney*, 1955]. The above hypotheses appear applicable to the ECS

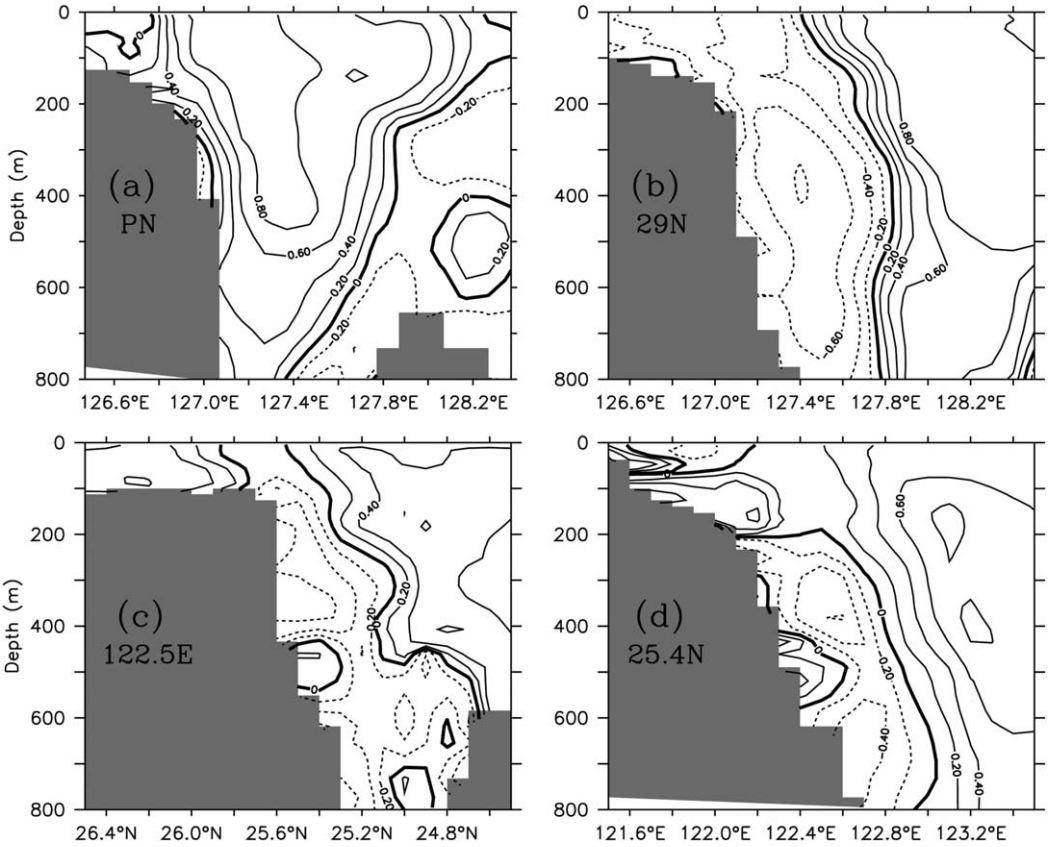

Figure 10. Correlation coefficients between the 1 year running mean KVT and the 1 year running mean cross-section velocity at (a) PN, (b) 29°N, (c) 122.5°E, and (d) 25.4°N sections. The 95% confidence level is ±0.18.

Kuroshio due to existence of the concave bathymetry structures; the Kuroshio is more inertia controlled so that it falls in the Charney regime and tends to flow in a strait path. A straight path that passes the shoreward concave isobaths of ECS shelf break, in particular immediately northeast of Taiwan and southwest of Kyushu (see Figure 1b for the bottom topography), means seaward deviation of the Kuroshio axis from the shelf break. Additionally, according to *Charney* [1955], the inertial western boundary thickness (Charney thickness or the characteristic width of the current) depends on velocity of the current, i.e., the higher the verlocity, the wider the region where nonlinearity is important, and the farther of the current axis away from the boundary. The seaward shift of the Kuroshio axis with an increase of KVT can be already deduced from Figures 9 and 10 in that the velocity of the Kuroshio is enhanced on the seaward side while it is either reduced or less enhanced on the shoreward side. Taking the horizontal position of the highest velocity at each depth layer as the index of the Kuroshio axis, we show the correlation of the Kuroshio axis change to KVT on interannual time scales in three typical sections: 123°E, PN and 129°E (Figure 11). The correlations suggest that increased KVT is accompanied by an offshore ward axis shift of the main Kuroshio stream at all depths (where the axis is significantly detected), and in all of the major intrusion regions (123°E), the separating region (PN section), and in the region away from the shelf (129°E, which is typical for studying the axis movement after the Kuroshio separates from the ECS shelf [*Sun and Su*, 1994; *Guo et al*., 2003]).

The seaward shift of a boundary current tends to create upwelling and cyclonic eddies on the shoreward side. *Wu et al*. [2008], based on high-resolution model results, argued that blocking of the Kuroshio by the zonally running shelf northeast of Taiwan causes the seaward deflection, and is ultimately responsible for the upwelling and cyclonic eddies. In addition, *Wu et al*. [2008] demonstrated that, on seasonal time scales, a seaward (shoreward) migration of the Kuroshio favors (suppresses) the formation of a cyclonic eddy. In the present study, the good consistency in spatial pattern between the Kuroshio axis and the occurrence or enhancement of the cyclonic eddies in the main intrusion and retreating regions, and over the entire ECS shelf break as shown in the composite map, confirms the tendency on interannual time scales.

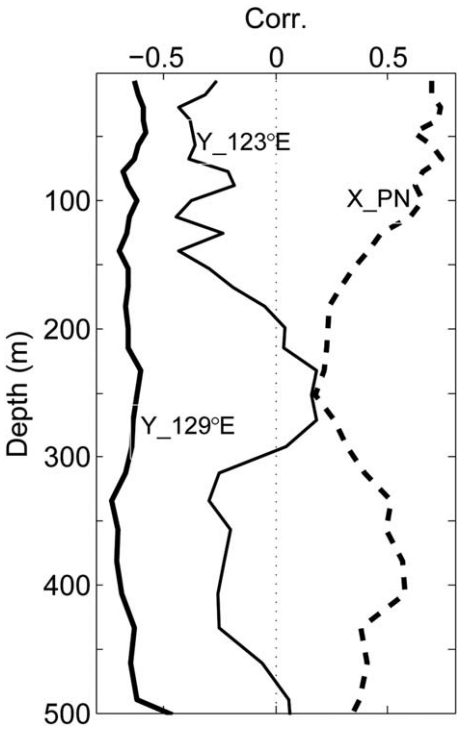

Figure 11. Correlation coefficients between the 1 year running mean KVT and the 1 year running mean Kuroshio axis at three sections on different levels. "X_PN" denotes that the axis at PN section is represented by its x (zonal) position, so as others.

The cyclonic eddy is accompanied with an upwelling-leading cold dome in upper depths. Figure 9 shows the temperature difference between the months of the highest and lowest 1 year running mean KVT at 80 m depth, where temperature varies largest (see below). It is clear that the cyclonic eddies at the major intrusion and retreating regions and the cyclonic recirculation along the entire ECS shelf break are accompanied by cold waters, occurring on the shoreward side of the mean Kuroshio path. The cold waters along the shelf break that are generated by the seaward shift of the mean Kuroshio current, which is further caused by the increase of KVT, are important to the KOI processes, i.e., in building the APV-JEBAR balance, a point we investigate in detail in the next section.

5.1.2. Changes of JEBAR Due to Occurrences of Cold Water

The seaward and shoreward flowing parts of the cyclonic eddies ultimately induced by the increase of KVT on interannual time scales are responsible for opposite signs of APV upstream and downstream; whereas the upwelling and cold water caused by the seaward shift of the Kuroshio axis result in local density structure change near the shelf break, which must be felt by the JEBAR term (see Appendix A). Since JEBAR is the dominant balancer of APV on large time scales, we may also use JEBAR to diagnose the Kuroshio intrusion processes, as was done in *Guo et al*. [2003] and *Oey et al*. [2010]. However, we note that the JEBAR pattern depends (partly) also on the current field so that it cannot by itself be used to explain the APV pattern; instead, it is more an indicator than a cause of the APV.

According to the definition of JEBAR in equation (A1), the horizontal gradient of potential energy X in the direction perpendicular to the isobaths does not generate net JEBAR; instead, only a gradient of X in the direction along the isobaths creates net JEBAR. To simplify the analysis, we rewrite the JEBAR term with a moving coordinate (n, l) as

$$J(X,h^{-1})=\frac{\partial X}{\partial l}\frac{\partial (h^{-1})}{\partial n}, \tag{1}$$

where n denotes the across-isobath direction pointing to the shallower water, l is 90° clockwise to n and parallel to isobaths. Because the second factor of the rhs term in equation (1) (relating to bottom depth gradient) is always positive, the sign of the first factor $\partial X/\partial l$ solely determines the sign of JEBAR (as well as APV). The 18 year averaged X along the 200 m isobath is shown in Figure 12a. The corresponding vertical structure of density along the 200 m isobath and the along isobath gradient of density, from which X is derived (vertically integrated), are shown in Figure 12b. It is seen that gradients of X along the isobaths always exist, suggesting that JEBAR plays an important role in balancing APV. X increases (decreases) along the 200 m isobath in intrusion (retreating) regions, which corresponds to a deepening (lifting) of isopycnals, or negative (positive) density gradients, respectively. This structure of X maintains the general pattern of APV (Figure 8a) and the cross-isobath volume transport (Figure 4a) of the 200 m isobath, which are

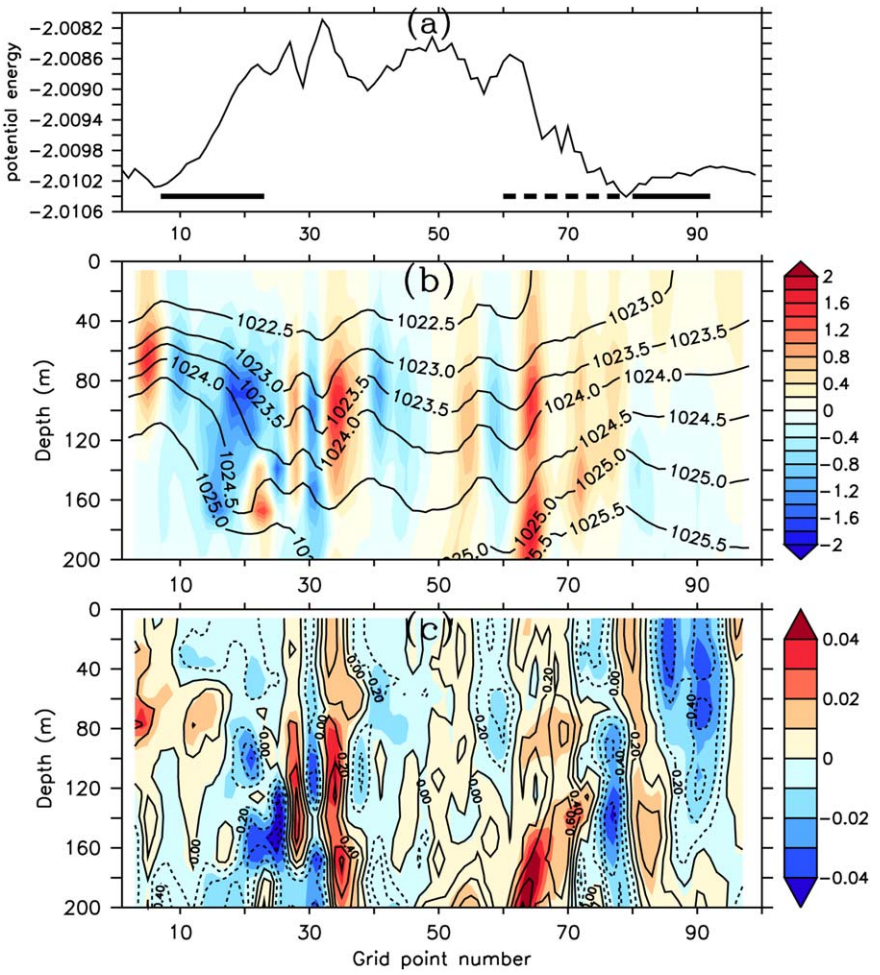

Figure 12. The 18 year (1993–2010) mean of (a) the potential energy X (see text; in 10^5 m^2 s^{-2}), (b) density (contours, in kg m^{-3}) and along isobath density gradient (colored, in kg m^{-4}) at each grid point along the 200 m isobath. (c) Correlation coefficients (contours) and regression coefficients (colored) between the 1 year running mean KVT and the 1 year running mean along isobath density gradient. The grid points are shown in Figure 1b. Thick lines (thick dotted line) at the bottom of Figure 12a denote intrusion (retreating) regions, same as those in Figure 4a.

characterized as intrusions upstream (points smaller than 35) and retreating downstream (points larger than 35) on the ECS shelf scale; therefore, the upside-down bowl-shaped X along the 200 m isobath shows up irrespective of time.

However, the strength of local $\partial X/\partial l$ varies interannually as a response to the KVT-induced cyclonic eddies and the associated upwelling and cold waters, which is shown in terms of correlation and regression coefficients between the 1 year running mean along-isobath density gradient and KVT (Figure 12c). For example, roughly southwest (northeast) of point 15, which is near the centers of the cyclonic eddy and cold water northeast of Taiwan (Figure 9), the along-isobath density gradient increases (decreases) with an increases of KVT. Point 15 might be considered as the turning point that divides the major intrusion region northeast of Taiwan into upstream and downstream regions. This division is most significantly found at 80 m, below or above which the turning point moves to the Taiwan coast. A similar pattern of increase (decrease) of along-isobath density gradient occurs southwest (northeast) of point 70 in the main retreating region. Though point 70 is not the center of the cyclonic eddy here at this depth, it is located at a local temperature minimum and separates the eddy into southwestward flowing and northeastward flowing flanks on its north and south sides, respectively (Figure 9). (Note Figure 12c shows that the most significant separation occurs below 80 m.) Another pair of increase/decrease of along-isobath density gradient happens in the other intrusion region in the whole column (points 79–93) where a cold center takes place.

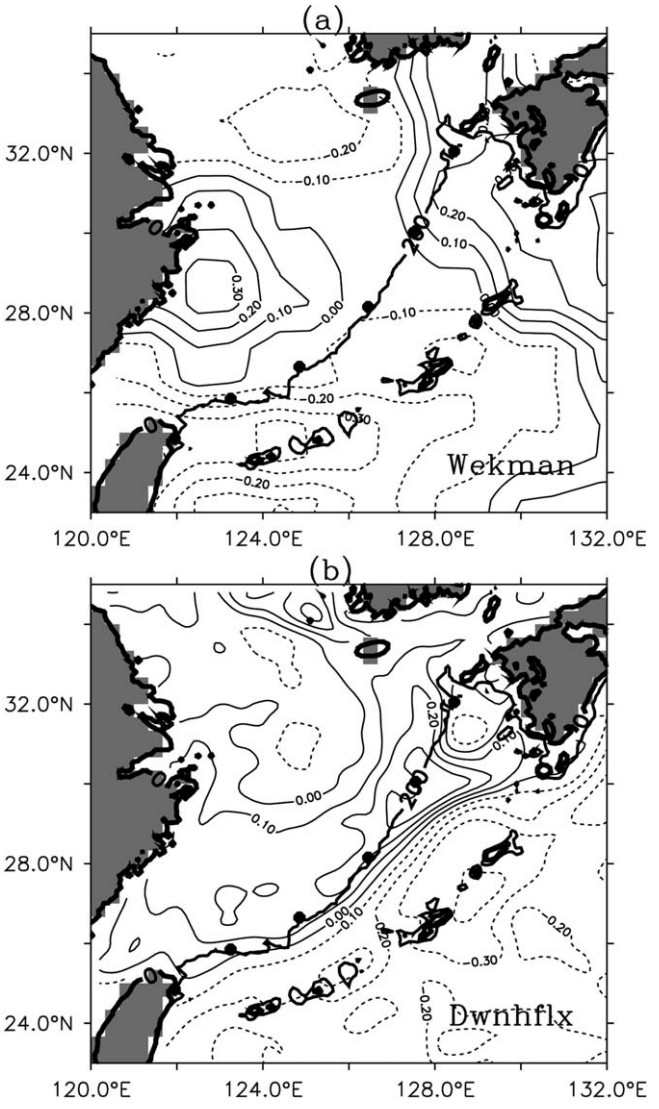

Figure 13. Correlation coefficients (thin contours) between the 1 year running mean KVT and the 1 year running mean (a) Ekman pumping velocity and (b) net downward heat flux. The thick line is the 200 m isobath. The Ekman pumping velocity, W_E, is calculated using $W_E = \frac{1}{\rho_0} curl_z\left(\frac{\tau_a}{f}\right)$. The wind stress and heat flux data are taken from NCEP/NCAR reanalysis [*Kalnay*, 1996].

Overall, we demonstrated in this section that when KVT increases, the changes of local KOI take place through the processes of the Kuroshio axis shift and generations of cyclonic eddies/upwelling. This causal relation is different from the causal relation at the seasonal scales, which has shown that the variations of the Kuroshio migration and KOI are caused by atmospheric induced, locally inhomogeneous cooling or heating. The latter causality needs to be taken into account or ruled out for interannual variations. To do this, we start from the general theory explaining the mean state of the Kuroshio intruding onto the shelf (northeast of Taiwan) given by *Stern and Austin* [1995]. The authors discussed that, as a portion of the Kuroshio intrudes onto the ECS shelf, compensating outflows with cyclonic vorticity cross the shelf break downward slope and are then entrained by the Kuroshio to maintain the free current in an "inertial boundary layer." This process results in the Kuroshio axis shifting with the strength of downward-slope vortex stretching: when the entrained vortex stretching is enhanced, it induces the same cyclonic vorticity to be produced on the cyclonic flank (from shoreward margin to the axis) of the Kuroshio over a shorter cross-slope distance, resulting in a thinner inertial boundary layer, and a Kuroshio axis that is closer to the shelf break.

A mechanism that can enhance the entrainment is the downward-slope sinking of wintertime colder water, which can be interpreted as the wintertime shoreward shift of the Kuroshio axis relative to the summer offshore movement of the Kuroshio axis [*Oey et al*., 2010]. If this local mechanism also works for the interannual variation, we would expect the generation of cold water on the shoreward side of the shelf break due to local atmospheric forces; however, we find this is not the case. The local atmospheric factor that affects temperature, the net downward surface heat flux, varies neither with the Kuroshio axis index used in Figure 11 (not shown), nor with the KVT (Figure 13b) in most of the study areas. In the region between points 50 and 90, the significant correlation only indicates that the atmosphere tends to heat the ocean, rather than cool it with the increase of KVT, which is not consistent with the result that the temperature of this region is cooled down with the increase of KVT (Figure 9).

Another local force that can analogously cause an axis shift of the Kuroshio is the Ekman pumping induced by local wind stress curl, which, however, is demonstrated below not to work in the current case, either. To take

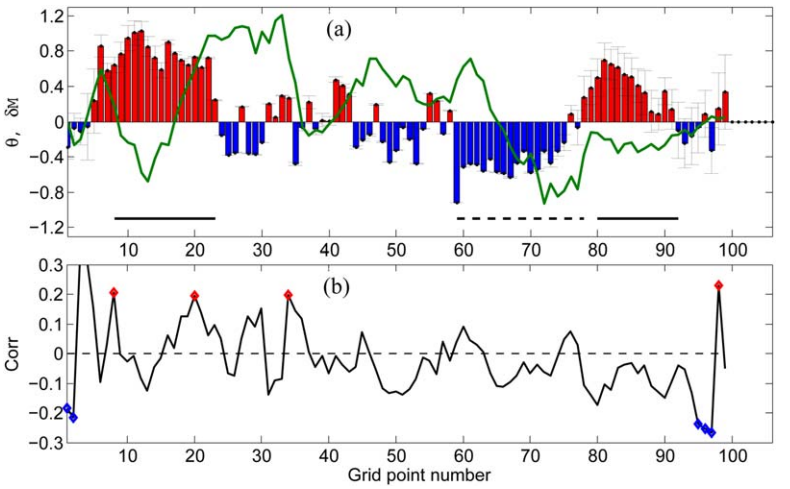

Figure 14. (a) The 18 year (1993–2010) mean θ (bars) and the STD (error bars) at each grid point along the 200 m isobath. The green line is the difference of the volume transport through a grid box (δM, see equation (4)) between months of highest and lowest 1 year running mean KVT. Thick lines (thick dotted line) at the bottom denote intrusion (retreating) regions, same as those in Figure 4a. (b) Correlation coefficient between the 1 year running mean θ at each grid point along the 200 m isobath and the 1 year running mean KVT. Points with red (blue) diamonds denote significant positive (negative) correlation over 95% confidence level. The grid points are shown in Figure 1b.

effect, an upward-slope upwelling of positive vorticity needs to be induced by the local wind stress curl in the cyclonic flank of the mean Kuroshio, which thereby causes upward-slope vortex *squeezing* in the shallower outer shelf and hence a longer cross-slope distance, resulting in a thicker inertial boundary layer of the Kuroshio and an off-shoreward axis shift. Therefore, Ekman pumping is required to be associated with increase of KVT on interannual time scales. However, correlation coefficients between the wind-induced Ekman pumping and KVT in the study region (Figure 13a) indicate that the wind will cause downwelling, rather than upwelling, northeast of Taiwan when KVT is higher than average. In addition, in the veering region, it does not show significant correlations with downwelling or upwelling. Another study [*Wu et al.*, 2008] also demonstrated that wind is not favorable for the upwelling northeast of Taiwan on seasonal and intraseasonal time scales.

5.2. A Diagnostic Interpretation on the Relation of KOI Locality to Local KVT

In the last subsection, we showed the correspondence of change of $\partial X/\partial l$ to KOI locality, based on which we will propose and test an explicit relation between KOI locality and local KVT in this section. The western boundary current is mainly characterized by an offshore-downward tilt of density isolines (Figure 2b). The along isobath gradient of X shown in Figure 13a is just one component of the total horizontal density gradient ∇X—the other component lies in the direction perpendicular to l. Therefore, there should be an angle θ between the gradient of h^{-1} and the gradient of mean X. Figures 13a and 13b implies that θ always exist and might not be small. Under this circumstance, the JEBAR term can be further rewritten in terms of the total horizontal gradient of X and θ as:

$$J(X,h^{-1})=|\nabla X|\sin(\theta)|\nabla h^{-1}|. \tag{2}$$

According to *Mertz and Wright* [1992, equation (9)], $\nabla X = hf\left(\bar{\boldsymbol{u}}_{\mathbf{p}}-\bar{\boldsymbol{u}}_{\mathbf{pb}}\right)$, where $\bar{\boldsymbol{u}}_{\mathbf{p}}$ and $\bar{\boldsymbol{u}}_{\mathbf{pb}}$ are the depth averaged geostrophic velocity and bottom geostrophic velocity, respectively. Taking into account that the current is in geostrophic balance and assuming that the bottom geostrophic velocity is small relative to the vertically averaged geostrophic velocity, ∇Xcan be written as $\nabla X \approx hf\bar{\boldsymbol{u}}_{\mathbf{p}}=f\mathbf{M}$, where $\mathbf{M}$ is the volume transport vector. Consequently, equation (2) is transformed to

$$J(X,h^{-1}) \approx |f\mathbf{M}|\sin(\theta)|\nabla h^{-1}|. \tag{3}$$

Considering the balance between APV and JEBAR, equation (3) suggests

$$KOI_{jebar} \sim fM\sin(\theta)|\nabla h^{-1}|, \tag{4}$$

in the northern hemisphere, M is the absolute value of $\mathbf{M}$. Equation (4) therefore establishes the relationship between local volume transport (not to be confused with KVT) and KOI. According to equation (4), KOI

changes with local volume transport in the presence of θ. θ ranges between 0 and $\pi/2$ when the Kuroshio approaches the isobaths (in an incident direction), e.g., in the region northeast of Taiwan, and between $-\pi/2$ and 0 when the Kuroshio leaves the shelf (like a reflection), e.g., in regions around PN and the eastern Taiwan coast. The existence of angle θ may play an important role in the local intrusion pattern, and was previously recognized in interpreting the bifurcation of Kuroshio both northeast of Taiwan and southwest of Kyushu [*Hsueh et al*., 1992, 1996]. (We note that one can also derive equation (4) in terms of APV in equation (A1), since the angel between gradient of h^{-1} and gradient of mean X is the same as the angel between directions of the mean geostrophic current and h^{-1} contours, as long as the current is geostrophic and the gradient of f is much smaller than that of h.)

The 18 year averaged θ and its STD along the 200 m isobath are shown in Figure 14a, which demonstrates that θ is nonzero and has weak STDs in most of the sections along the shelf break (between points 6 and 85) on interannual time scales. In addition, θ almost does not change with KVT (Figure 14b), meaning that even though the Kuroshio axis shifts seaward or shoreward, the incident or reflecting angle relative to the isobaths will not change. The result of steady θ is interesting, and is indicated by a laboratory study of nonlinear Western Boundary Currents [*Pierini et al*., 2011. Pierini et al. found that either in a highly nonlinear inertial Charney regime or in a weakly nonlinear regime, a notable increase of the current speed does not change the direction of it. Therefore, it becomes not surprising that θ is not changing with KVT when the ECS Kuroshio does not experience transition from one regime to another during the study period (it might fall into the Charney regime like the Gulf Stream [*Charney*, 1955]). θ is largest in magnitude in the major intrusion region and in the main retreating region, which is because that the Kuroshio passes the concave isobaths upstream of the major intrusion region and downstream of the main separating region due to inertia, respectively. In the major intrusion regions northeast of Taiwan (points 8–23) and the main retreating regions (points 59–80), θ ranges between $\pi/5$ and $\pi/3$ and between $-\pi/7$ and $-\pi/5$, respectively.

To compare how well the diagnostic estimation equation (4) is able to represent the APV or KOI fluxes, we show KOI_{jebar} in Figure 4a overlaying on true KOI. Note that in Figure 4a, KOI_{jebar} has a same dimension as APV and is scaled by $0.02 \times (KOI_{jebar})^{0.6}$ to match the axis range. Clearly, KOI_{jebar} resembles the cross-200 m isobath volume transport, particularly in the intrusion and separation regions. Since θ is stable on interannual time scales, the interannual variation of KOI_{jebar} is therefore dominated by that of M at a certain point. δM, the difference of M between months of highest and lowest KVT (Figure 14a), decreases and increases upstream (points 9–16) and downstream (points 17–23), respectively, of the major intrusion region northeast of Taiwan. This is because that these two areas correspond with the southward and northward flowing parts of the cyclonic eddy-like difference (Figure 9), resulting from a decrease and increase to the northeastward flowing mean current, respectively, as a consequence of seaward axis shift. Since θ is steadily positive, the negative (positive) anomalies of M results in negative (positive) correlations between KOI and KVT, consistent with the conclusions in section 4. An analogous conclusion can be reached in the veering region (points 59–79). However, this conclusion becomes problematic north of point 85, where the STD of θ becomes so large that θ may change sign with time.

6. Conclusions and Discussions

Using simulations of a high-resolution and real-time ocean general circulation model, we investigated the interannual variability of the KVT in the ECS and KOI along the ECS shelf break in the years 1993–2010. The 18 year averaged Kuroshio onshore flux across the 200 m isobath is 0.87 Sv and the STD of the 1 year running mean is 0.24 Sv. During this period, both KVT and the total cross-200 m isobath volume transport show interannual variability on time scales of $\sim$4 year period. The interannual variability takes place mainly in the major intrusion region northeast of Taiwan and the main veering region where the Kuroshio separates from the ECS shelf break. Obvious interannual, in-phase covariation is found between KVT and the total cross-200 m isobath KOI.

KVT also influences the local pattern of the KOI along the shelf break on interannual time scales. When KVT increases, the intrusion decreases upstream, but increases downstream of the major intrusion region northeast of Taiwan. On the contrary, the retreating is enhanced upstream and reduced downstream of the main retreating region. The different behaviors between upstream and downstream are caused by the generation

of surface reaching cyclonic eddies and the corresponding upwelling and cold water in between the upstream and downstream regions. In turn, the generation of cyclonic eddies are due to deviation of the Kuroshio axis from the shelf, which is further caused by the increase of KVT under effect of inertia. The effect of nonlinear inertial term might be directly tested in the future. The interannual deviation of Kuroshio axis not only induces mesoscale cyclonic eddy-like velocity differences in the two major seaward turning regions, but also induces a shelf-scale cyclonic recirculation-like velocity difference that flows around the shoreward margin of the Kuroshio.

A diagnostic mechanism equation (4) is proposed to interpret the relation between KVT and KOI with respect to both the mean state and the interannual variations. Equation (4) is derived from the preliminary two-factor balance between APV and JEBAR of the across isobaths transport. The angle θ between the mean current and topography, which is relatively stable on interannual time scales and determined primarily by the properties of the Kuroshio (such as competition of inertia and PV conservation) and the local bottom topography, plays an crucial role in establishing the relation between KVT and KOI. The sign of θ determines the intruding or retreating pattern of the mean Kuroshio along the shelf break, while the strength of volume transport along the shelf break determines the strength of intrusion or retreatment. When the local volume transport is increased (corresponding to regions that are downstream of the major intrusion region northeast of Taiwan and upstream of the main separating region southwest of Kyushu), more intrusion (retreating) will take place if θ is positive (negative). Since θ is stable on interannual time scales, the local pattern of the interannual variability of KOI is mostly determined by *M*.

The mechanism of interannual variation of KOI revealed here is different from that on the seasonal time scales. *Oey et al*. [2010] and *Guo et al*. [2003] demonstrated that the local atmospheric factor (local warming and cooling) is responsible for the seasonal variation. In that case, APV, a property of current field, adjusts with spatial variations of density field (JEBAR). In the case of interannual variability, we do not find relations of local surface heat fluxes or wind to the APV or KOI; instead, we find that the interior Pacific born remote factor, KVT, highly determines the local APV pattern through the Kuroshio axis shift. In this scenario, upwelling and the associated cold water are generated in the cyclonic flank of the Kuroshio due to fluctuation of KVT, meaning that a net JEBAR is produced as a response to current, or APV changes. The effect of KVT on KOI might also be applicable to the seasonal variation: the KVT is generally high (low) in summer (winter), which is accompanied by seaward (shoreward) shift of axis and more often appearance of cyclonic eddies.

The effect of interannual variation of the KVT on the Kuroshio intrusion onto the ECS shelf is not limited to the shelf break regions. Figures 8 and 9 clearly suggest that the interannual variation of KVT is accompanied by changes of the entire ECS shelf circulations, especially in the Taiwan Strait and Tsushima Warm Current source region. The influence seems also to reach the northern ECS [e.g., *Yang et al*., 2011, 2012]. However, the questions of how the KVT affects the entire ECS circulation, and whether the circulation changes are consequence of the changing KVT as a sole factor, or whether they are simultaneous consequence of other independent factors, go beyond the scope of this study. We only note that the volume transport through the entire Taiwan Strait is positively correlated with KVT on interannual time scales (correlation coefficient $+0.75$); by contrary, the volume transport through the entire Tsushima Strait is not (Figure 6), though in the source region of Tsushima Current it is negatively related to KVT. Nevertheless, their influences on the ECS circulations should be coupled to each other and need further studies.

The interannual variation of KVT in the ECS might also affect the bimodality of Kuroshio path south of Japan. The latter has been considered as a hysteresis phenomenon controlled by the upstream inflow fluctuations of volumes and path positions [e.g., *Chao*, 1984], though the relation is subtle [*Kawabe*, 1995]. We noticed that with increase of KVT the Kuroshio shifts seaward from the Kyushu coast east of 131°E (Figure 9). By contrary, a hypothesis that the existence of a self-sustained mechanism in the Kuroshio Current system can generate bimodal path variations on an interannual time scale [*Qiu and Miao*, 2000] is widely recognized. While quantifying the mechanisms is beyond the scope of this study, it would be of interest to employ this issue using the STORM data.

Appendix A: APV and TPV

A vorticity equation is obtained by vertically averaging the linearized momentum equations first and then taking a curl [*Guo et al.*, 2003]:

$$\underbrace{\frac{\partial}{\partial t} curl_z\left(\frac{\mathbf{M}}{h}\right)}_{I} + \underbrace{\mathbf{M}\cdot\nabla\left(\frac{f}{h}\right)}_{II} = \underbrace{J(X,h^{-1})}_{III} + \underbrace{curl_z\left(\frac{\boldsymbol{\tau}_a}{\rho_0 h}\right)}_{IV} \underbrace{-curl_z\left(\frac{\boldsymbol{\tau}_b}{\rho_0 h}\right)}_{V} + \underbrace{curl_z\left(\frac{\mathbf{D}}{h}\right)}_{VI} - \underbrace{curl_z\left(\frac{\mathbf{A}}{h}\right)}_{VII}, \tag{A1}$$

where $J(A,B)=\frac{\partial A}{\partial x}\frac{\partial B}{\partial y}-\frac{\partial A}{\partial y}\frac{\partial B}{\partial x}$ is the Jacobian operator, $X=\int_{-h}^{0} zg\rho/\rho_0 dz$ the potential energy, f the Coriolis parameter, h the bottom depth, ∇ the horizontal gradient operator, $\mathbf{M}=\int_{-h}^{0}\vec{\boldsymbol{u}}dz$ the transport vector, $\vec{\boldsymbol{u}}$ the velocity vector, g the gravitational acceleration, ρ and ρ_0 the potential density and its background, respectively. Term (I) is neglected when one considers a quasi-steady state of the Kuroshio. Term (III) is JEBAR; Terms (IV) and (V) are the curls of wind stress τ_a and bottom stress τ_b modified by depth, respectively. Terms (VI) and (VII) are the curls of vertically averaged horizontal diffusion term (**D**) and nonlinear advection term (**A**), respectively. Term (II) is APV, which stands for advection of potential vorticity, and clearly displays the volume transport across the *f/h* contours [*Mertz and Wright*, 1992]: if APV = 0, the transport is exactly along the *f/h* contours and no transport across *f/h* contours is generated; if APV > 0 (<0), the transport flows in the onshore (offshore) direction and the Kuroshio tends toward the ECS shelf (Okinawa Trough). Since gradient of *f* is smaller than that of *h*, especially over the shelf break region, APV becomes the indicator of cross-isobaths transport. The long-term averaged APV—that is proportional to the long-term averaged Kuroshio onshore flux—is primarily balanced by the JEBAR term at each fixed point along the shelf break; in addition, variation of APV is also primarily balanced by variation of JEBAR on seasonal [see *Guo et al.*, 2006] and interannual time scales (not shown). These balances indicate that the Kuroshio onshore transport across the ECS shelf break is basically in a geostrophic state. The wind stress curl terms and other terms contribute much less to the local vorticity balance in either long-term mean or seasonal to interannual variations.

In analogy, TPV, a counterpart of APV, which presents volume transport *along* the *f/h* contours, is defined as

$$\mathrm{TPV}=\mathbf{M}\cdot\nabla_{\perp}\left(\frac{f}{h}\right), \tag{A2}$$

where $\nabla_{\perp}=\mathbf{k}\times\nabla$ denotes anticlockwise rotation of the horizontal gradient by 90°, **k** is the vertical unit. TPV is positive (negative) when the vertically integrated current **M** flows along the *f/h* contours with larger depth on the right (left) side.

Acknowledgments

This work is supported by the "Strategic Priority Research Program" of the Chinese Academy of Sciences (XDA11010201 and XDA11020104). The STORM model was run at the German high-performance computing center DKRZ. We are grateful to Mark Carson for his English proofreading. We would also like to thank the two anonymous reviewers whose comments helped to improve the manuscript.

Reference

Akimoto, K., M. Ooi, T. Awaji, and K. Kutsuwada (1996), Interannual variability of the Kuroshio transport in response to the wind stress field over the North Pacific: Its relation to the path variation south of Japan, *J. Geophys. Res.*, *101*, 14,057–14,071, doi:10.1029/96JC01000.

Chang, Y.-L., and L.-Y. Oey (2011), Interannual and seasonal variations of Kuroshio transport east of Taiwan inferred from 29 years of tide-gauge data, *Geophys. Res. Lett.*, *38*, L08603, doi:10.1029/2011GL047062.

Chao, S. Y. (1984), Bimodality of the Kuroshio, *J. Phys. Oceanogr.*, *14*, 92–103.

Charney, J. G. (1955), The Gulf Stream as an inertial boundary layer, *Proc. Natl. Acad. Sci. U. S. A.*, *41*, 731–740.

Chen, C., R. C. Beardsley, and R. Limeburner (1992), The structure of the Kuroshio southwest of Kyushu: Velocity, transport, and potential vorticity fields, *Deep Sea Res., Part A*, *39*, 245–268.

Chen, C. T. A. (1996), The Kuroshio intermediate water is the major source of nutrients on the East China Sea continental shelf, *Oceanol. Acta*, *5*, 523–527.

Chuang, W. S., and W. D. Liang (1994), Seasonal variability of intrusion of the Kuroshio water across the continental shelf northeast of Taiwan, *J. Oceanogr.*, *50*, 531–542.

Chuang, W. S., H. W. Li, Y. T. Tang, and C. K. Wu (1993), Observations of the countercurrent on the inshore side of the Kuroshio northeast of Taiwan, *J. Oceanogr.*, *49*, 581–592.

Feng, M., H. Mitsudera, and Y. Yoshikawa (2000), Structure and variability of the Kuroshio Current in the Tokara Strait, *J. Phys. Oceanogr.*, *30*, 2257–2276.

Gilson, J., and D. Roemmich (2002), Mean and temporal variability in Kuroshio geostrophic transport south of Taiwan (1993–2001), *J. Oceanogr.*, *58*, 183–195.

Guo, X., H. Hukuda, Y. Miyazawa, and T. Yamagata (2003), A triply nested ocean model for simulating the Kuroshio–Roles of horizontal resolution on JEBAR, *J. Phys. Oceanogr.*, *33*, 146–169.

Guo, X., Y. Miyazawa, and T. Yamagata (2006), The Kuroshio onshore intrusion along the shelf break of the East China Sea: The origin of the Tsushima Warm Current, *J. Phys. Oceanogr.*, *36*, 2205–2231.

He, Y., and W. B. White (1987), Interannual variability of the Kuroshio frontal structure along its western boundary in the North Pacific ocean associated with the 1982 ENSO event, *J. Phys. Oceanogr.*, *17*, 1494–1506.

Hinata, T. (1996), Seasonal variation and long-term trends of the oceanographic conditions along a fixed hydrographic line crossing the Kuroshio in the East China Sea, *Oceanogr. Mag.*, *45*, 9–32.
Hsueh, Y. (2000), The Kuroshio in the East China Sea, *J. Mar. Syst.*, *24*, 131–139.
Hsueh, Y., J. Wang, and C. S. Chern (1992), The intrusion of the Kuroshio across the continental shelf northeast of Taiwan, *J. Geophys. Res.*, *97*, 14,323–14,330.
Hsueh, Y., C.-S. Chern, and J. Wang (1993), Blocking of the Kuroshio by the continental shelf northeast of Taiwan, *J. Geophys. Res.*, *98*, 12,351–12,359.
Hsueh, Y., H.-J. Lie, and H. Ichikawa (1996), On the branching of the Kuroshio west of Kyushu, *J. Geophys. Res.*, *101*, 3851–3857.
Hwang, C., and R. Kao (2002), TOPEX/POSEIDON-derived space–time variations of the Kuroshio current: Applications of a gravimetric geoid and wavelet analysis, *Geophys. J. Int.*, *151*, 835–847.
Ichikawa, H., and M. Chaen (2000), Seasonal variation of heat and freshwater transports by the Kuroshio in the East China Sea, *J. Mar. Syst.*, *24*, 119–129.
Ichikawa, H., and R. C. Beardsley (1993), Temporal and spatial variability of volume transport of the Kuroshio in the East China Sea, *Deep Sea Res., Part I*, *40*, 583–605.
Ichikawa, K. (2001), Variation of the Kuroshio in the Tokara Strait induced by meso-scale eddies, *J. Oceanogr.*, *57*, 55–68.
Isobe, A. (1999), On the origin of the Tsushima Warm Current and its seasonality, *Cont. Shelf Res.*, *19*, 117–133.
Isobe, A. (2008), Recent advances in ocean-circulation research on the Yellow Sea and East China Sea shelves, *J. Oceanogr.*, *64*, 569–584.
Ito, T., A. Kaneko, H. Furukawa, N. Gohda, and W. Koterayama (1995), A structure of the Kuroshio and its related upwelling on the East China Sea shelf slope, *J. Oceanogr.*, *51*, 267–278.
Jungclaus, J. H., N. Keenlyside, M. Botzet, H. Haak, J.-J. Luo, M. Latif, J. Marotzke, U. Mikolajewicz, and E. Roeckner (2006), Ocean circulation and tropical variability in the coupled ECHAM5/MPI-OM, *J. Clim.*, *19*, 3952–3972.
Kalnay, E., et al. (1996), The NCEP/NCAR Reanalysis 40-year Project, *Bull. Am. Meteorol. Soc.*, *77*, 437–471.
Kawabe, M. (1995), Variations of current path, velocity, and volume transport of the Kuroshio in relation with the large meander, *J. Phys. Oceanogr.*, *25*, 3103–3117.
Lee, J.-S., and T. Matsuno (2007), Intrusion of Kuroshio water onto the continental shelf of the East China Sea, *J. Oceanogr.*, *63*, 309–325.
Liang, W. D., T. Y. Tang, Y. J. Yang, M. T. Ko, and W. S. Chuang (2003), Upper ocean currents around Taiwan, *Deep Sea Res., Part II*, *50*, 1085–1105.
Lie, H., C. Cho, J. Lee, P. Niiler, and J. Hu (1998), Separation of the Kuroshio water and its penetration onto the continental shelf west of Kyushu, *J. Geophys. Res.*, *103*, 2963–2976, doi:10.1029/97JC03288.
Liu, K. K., G. C. Gong, S. Lin, C. Y. Yang, C. L. Wei, S. C. Pai, and C. K. Wu (1992), The year-round upwelling at the shelf break near the northern tip of Taiwan as evidenced by chemical hydrography, *Terr. Atmos. Oceanic Sci.*, *3*, 243–276.
Mertz, G., and D. G. Wright (1992), Interpretations of the JEBAR Term, *J. Phys. Oceanogr.*, *22*, 301–305.
Nitani, H. (1972), Beginning of the Kuroshio, in *Kuroshio, Physical Aspects of the Japan Current*, edited by H. Stommel and K. Yoshida, pp. 129–164, Univ. of Wash. Press, Seattle.
Oey, L.-Y., Y.-C. Hsin, and C.-R. Wu (2010), Why does the Kuroshio northeast of Taiwan shift shelfward in winter?, *Ocean Dyn.*, *60*, 413–426.
Pierini, S., P. Falco, G. Zambardino, T. A. McClimans, and I. Ellingsen (2011), A laboratory study of nonlinear western boundary currents, with application to the Gulf Stream separation due to inertial overshooting, *J. Phys. Oceanogr.*, *41*, 2063–2079.
Qiu, B., and S. Chen (2010), Interannual variability of the North Pacific STCC and its associated mesoscale eddy field, *J. Phys. Oceanogr.*, *40*, 213–225, doi:10.1175/2009JPO4285.1.
Qiu, B., and N. Imasato (1990), A numerical study on the formation of the Kuroshio counter current and the Kuroshio branch current in the East China Sea, *Cont. Shelf Res.*, *10*, 165–184.
Qiu, B., and W. Miao (2000), Kuroshio path variations south of Japan: Bimodality as a self-sustained internal oscillation, *J. Phys. Oceanogr.*, *30*, 2124–2137.
Saiki, M. (1982), Relation between the geostrophic flux of the Kuroshio in the Eastern China Sea and its large meandering south of Japan, *Oceanogr. Mag.*, *32*, 11–18.
Sarkisyan, S., and V. F. Ivanov (1971), Joint effect of baroclinicity and bottom relief as an important factor in the dynamics of sea currents, *Izv. Acad. Sci. USSR Atmos. Oceanic Phys., Engl. Transl.*, *7*, 173–188.
Sheremet, V. A. (2001), Hysteresis of a western boundary current leaping across a gap, *J. Phys. Oceanogr.*, *31*, 1247–1259.
Stern, M., and J. Austin (1995), Entrainment of shelf water by a bifurcating continental boundary current, *J. Phys. Oceanogr.*, *25*, 3118–3131.
Su, J. L., B. X. Guan, and J. Z. Jiang (1990), The Kuroshio. Part I. Physical features, *Oceanogr. Mar. Biol. Annu. Rev.*, *28*, 11–71.
Sun, X. (1987), Analysis of the surface path of the Kuroshio in the East China Sea, in *Essays on Investigation of Kuroshio*, pp. 1–14, China Ocean Press, Beijing, China.
Sun, X.-P., and Y.-F. Su (1994), On the variation of Kuroshio in East China Sea, in *Oceanology of China Seas*, vol. 1, edited by D. Zhou, Y.-B. Liang, and C. K. Tseng, pp. 49–58, Kluwer Acad, Dordrecht, Netherlands.
Tang, T. Y., and Y. J. Yang (1993), Low frequency current variability on the shelf break northeast of Taiwan, *J. Oceanogr.*, *49*, 193–210.
Tang, T. Y., Y. Hsueh, Y. J. Yang, and J. C. Ma (1999), Continental slope flow northeast of Taiwan, *J. Phys. Oceanogr.*, *29*, 1353–1362.
Tang, T. Y., J. H. Tai, and Y. J. Yang (2000), The flow pattern north of Taiwan and the migration of the Kuroshio, *Cont. Shelf Res.*, *20*, 349–371.
Teague, W. J., G. A. Jacobs, H. T. Perkins, J. W. Book, K. I. Chang, and M.-S. Suk (2002), Low frequency current observations in the Korea/Tsushima Strait, *J. Phys. Oceanogr.*, *32*, 1621–1641.
Teague, W. J., G. A. Jacobs, D. S. Ko, T. Y. Tang, K. I. Chang, and M.-S. Suk (2003), Connectivity of the Taiwan, Cheju, and Korea straits, *Cont. Shelf Res.*, *23*, 63–77.
Torrence, C., and G. P. Compo (1998), A practical guide to wavelet analysis, *Bull. Am. Meteorol. Soc.*, *79*, 61–78.
Vallis, G. K. (2006), *Atmospheric and Oceanic Fluid Dynamics*, 603 pp., Cambridge Univ. Press, Cambridge, U. K.
von Storch, J.-S., C. Eden, I. Fast, H. Haak, D. Hernández-Deckers, E. Maier-Reimer, J. Marotzke, and D. Stammer (2012), An estimate of the Lorenz energy cycle for the World Ocean based on the STORM/NCEP simulation, *J. Phys. Oceanogr.*, *42*, 2185–2205, doi:10.1175/JPO-D-12-079.1.
Wong, G. T. F., S.-Y. Chao, Y.-H. Li, and F.-K. Shiah (2000), The Kuroshio edge exchange processes (KEEP) study—An introduction to hypotheses and highlights, *Cont. Shelf Res.*, *20*, 335–347.
Wu, C.-R., H.-F. Lu, and S.-Y. Chao (2008), A numerical study on the formation of upwelling off northeast Taiwan, *J. Geophys. Res.*, *113*, C08025, doi:10.1029/2007JC004697.

Yamagata, T., Y. Shibao, and S. Umatani (1985), Interannual variability of the Kuroshio extension and its relation to the Southern Oscillation/El Nifio, *J. Oceanogr. Soc. Jpn.*, *41*,274–281.

Yang, D., B. Yin, Z. Liu, and X. Feng (2011), Numerical study of the ocean circulation on the East China Sea shelf and a Kuroshio bottom branch northeast of Taiwan in summer, *J. Geophys. Res.*, *116*, C05015, doi:10.1029/2010JC006777.

Yang, D., B. Yin, Z. Liu, T. Bai, J. Qi, and H. Chen (2012), Numerical study on the pattern and origins of Kuroshio branches in the bottom water of southern East China Sea in summer, *J. Geophys. Res.*, *117*, C02014, doi:10.1029/2011JC007528.

Zhang, D., T. N. Lee, W. E. Johns, C. T. Liu, and R. Zantopp (2001), The Kuroshio east of Taiwan: Modes of variability and relationship to interior ocean mesoscale eddies, *J. Phys. Oceanogr.*, *31*, 1054–1074.

Zhang, Q., Y. Hou, and T. Yan (2012), Inter-annual and inter-decadal variability of Kuroshio heat transport in the East China Sea, *Int. J. Climatol.*, *32*, 481–488, doi:10.1002/joc.2295.